Late-Onset Inner Retinal Dysfunction in Mice Lacking Sigma Receptor 1 (σR1)

Yonju Ha,[1,2] *Alan Saul,*[2,3] *Amany Tawfik,*[1,2] *Cory Williams,*[1,2] *Kathryn Bollinger,*[2,3] *Robert Smith,*[1] *Masanori Tachikawa,*[4] *Eric Zorrilla,*[5] *Vadivel Ganapathy,*[2,6] *and Sylvia B. Smith*[1,2,3]

Purpose. Sigma receptor 1 (σR1) is expressed abundantly in the eye, and several reports suggest that this putative molecular chaperone plays a role in lens cell survival, control of intraocular pressure (IOP), and retinal neuroprotection. The present study examined the consequence of the absence of σR1 on ocular development, structure, and function.

Methods. Wild-type ($\sigma R1^{+/+}$), heterozygous ($\sigma R1^{+/-}$), and homozygous ($\sigma R1^{-/-}$, knockout) mice aged 5 to 59 weeks were subjected to comprehensive electrophysiological testing and IOP measurement. The eyes were examined by light and electron microscopy and subjected to morphometric examination and detection of apoptosis.

Results. Cornea and lens of $\sigma R1^{-/-}$ mice were similar to wild-type mice in morphologic appearance at all ages examined, and IOP was within normal limits. Comprehensive ERG and morphometric analyses initially yielded normal findings in the $\sigma R1^{-/-}$ mice compared with those in the wild-type. By 12 months, however, significantly decreased ERG b-wave amplitudes and diminished negative scotopic threshold responses, consistent with inner retinal dysfunction, were detected in $\sigma R1^{-/-}$ mice. Concomitant with these late-onset changes were increased TUNEL- and active caspase 3-positive cells in the inner retina and significant loss of cells in the ganglion cell layer, particularly in the central retina. Before these functional and structural abnormalities, there was ultrastructural evidence of axonal disruption in the optic nerve head of $\sigma R1^{-/-}$ mice as early as 6 months of age, although there were no alterations observed in retinal vascularization in $\sigma R1^{-/-}$ mice.

Conclusions. These data suggest that lack of σR1 leads to development of late-onset retinal dysfunction with similarities to optic neuropathy. (*Invest Ophthalmol Vis Sci.* 2011;52: 7749–7760) DOI:10.1167/iovs.11-8169

From the Departments of [1]Cellular Biology and Anatomy, [3]Ophthalmology, and [6]Biochemistry and Molecular Biology, and the [2]Vision Discovery Institute, Medical College of Georgia, Georgia Health Sciences University, Augusta, Gerogia; the [4]Department of Pharmaceutics, University of Toyama, Toyama, Japan; and the [5]Harold L. Dorris Neurological Research Institute, The Scripps Research Institute, La Jolla, California.

Supported by National Institutes of Health Grant R01 EY014560.

Submitted for publication July 5, 2011; revised August 11, 2011; accepted August 11, 2011.

Disclosure: **Y. Ha**, None; **A. Saul**, None; **A. Tawfik**, None; **C. Williams**, None; **K. Bollinger**, None; **R. Smith**, None; **M. Tachikawa**, None; **E. Zorrilla**, None; **V. Ganapathy**, None; **S.B. Smith**, None

Corresponding author: Sylvia B. Smith, Department of Cellular Biology and Anatomy, Medical College of Georgia, Georgia Health Science University, 1120 15th Street, CB 2901, Augusta, GA 30912-2000; sbsmith@georgiahealth.edu.

Sigma receptor 1 (σR1) is a transmembrane protein associated with the endoplasmic reticulum (ER). It modulates many signal transduction events within cells and may operate as a unique ligand-regulated molecular chaperone at the ER–mitochondrion membrane (MAM).[1] In the eye, σR1 is expressed in lacrimal gland, cornea, iris-ciliary body, lens, and retina.[2–4] Modulating σR1 activity lowers intraocular pressure in vivo.[4,5] Antagonizing σR1 in vitro, either pharmacologically or with siRNA, inhibits lens cell growth, increases lens cell death, and leads to accumulation of pigment granules in the lens.[6,7] In the retina, σR1 is expressed abundantly in the ganglion cell layer (GCL), cells of the inner nuclear layer (INL), photoreceptor cells, the RPE, and optic nerve.[8–11] In retinal Müller and ganglion cells (RGCs), immunolocalization studies detect σR1 on the ER and nuclear membranes.[12,13] The σR1-specific ligand (+)-pentazocine ((+)-PTZ) protects against oxidative stress–induced RGC death in vitro[14,15]; in vivo, it prevents loss of RGCs and disruption of the inner retina of diabetic $Ins2^{Akita/+}$ mice.[16] Mechanisms suggested for retinal neuroprotection by σR1 ligands include regulation of intracellular Ca^{2+} levels and attenuation of proapoptotic gene activation,[17] suppression of NMDA-receptor–mediated current responses in ON- and OFF-ganglion cells,[18] and increased binding of σR1 to the key ER chaperone protein BiP/glucose-regulated protein 78 (BiP/Grp78).[13]

The consequences of absence of σR1 on ocular phenotype have not been investigated, but the availability of genetically manipulated mice lacking $\sigma R1$ ($\sigma R1^{-/-}$ mice) offers a tool to clarify the role of σR1 in ocular development and disease. Given its abundant expression in the eye, its role in neuroprotection and cell survival, and its putative molecular chaperone role, we postulated that σR1 would be critical for ocular development and/or maintenance of normal ocular structure/function. To test this, we used functional, morphologic, and cell biological tools to examine comprehensively the ocular phenotype in $\sigma R1^{-/-}$ versus $\sigma R1^{+/+}$ mice over a 1-year period. Our data show that the anterior segment of the eye (cornea, lens, and ciliary body-iris) is normal in $\sigma R1^{-/-}$ mice and intraocular pressure (IOP) is within normal limits at all ages examined. In the retina, however, there are electrophysiological changes in $\sigma R1^{-/-}$ mice including significantly decreased ERG b-wave amplitudes and diminished negative scotopic threshold responses detected at 12 months, consistent with inner retina dysfunction. Morphologic analyses reveal significantly fewer cells in the GCL. There is ultrastructural evidence of disruption of axons of the optic nerve head (ONH) including accumulation of organelles (swollen mitochondria) and glial cell apoptosis. The data suggest that σR1 is critical in maintaining inner retinal function. Investigations of this molecular chaperone may provide important insights into retinal diseases associated with optic nerve disruption and RGC loss.

METHODS

Animals

One hundred eighteen mice were used in the study (Table 1). The $\sigma R1^{-/-}$ mice were generated by gene trapping ($Oprs1^{Gt(IRESBetageo)33Lex}$/$Oprs1^{Gt(IRESBetageo)33Lex}$) conducted at Lexicon Genetics Corp. (The Woodlands, TX; http://www.informatics.jax.org/searches/accession_report.cgi?id=MGI:3529055). Heterozygote Oprs1 mutant (+/−) $Oprs1^{Gt(IRESBetageo)33Lex}$ embryos on a C57BL/6J × 129S/SvEv mixed background were obtained from the Mutant Mouse Resource Regional Center and implanted into female C57BL/6J mice (Jackson Laboratories, Bar Harbor, ME) at The Scripps Research Institute. Founder heterozygous mice were transferred to the animal facility at Georgia Health Sciences University, and colonies of wild-type ($\sigma R1^{+/+}$), heterozygous ($\sigma R1^{+/-}$), and homozygous ($\sigma R1^{-/-}$) mice were established. Genotyping of mice was performed as described.[19] Maintenance of the animals adhered to institutional guidelines for humane treatment of animals and to the ARVO Statement for Use of Animals in Ophthalmic and Vision Research.

σR1 Gene Expression Analysis

Neural retina, RPE/eyecup, brain, kidney, and liver were harvested from $\sigma R1^{+/+}$, $\sigma R1^{+/-}$, and $\sigma R1^{-/-}$ mice. Expression of mRNA transcripts for *σR1* was examined by semiquantitative RT-PCR by our method.[13] Primer pairs used for *σR1* and *18S* (control) have been described.[13]

Western Blot Analysis

Neural retina and brain were harvested from $\sigma R1^{+/+}$, $\sigma R1^{+/-}$, and $\sigma R1^{-/-}$ mice. Proteins were isolated and subjected to SDS-PAGE as described.[16] Nitrocellulose membranes, to which the separated proteins had been transferred, were incubated with a primary antibody against σR1[9] (1:400) and were then incubated with HRP-conjugated goat anti-rabbit IgG antibody (1:3000; Santa Cruz Corp., Santa Cruz, CA). Proteins were visualized using a chemiluminescent detection system (SuperSignal West Pico Chemiluminescent Substrate; Pierce Biotechnology, Rockford, IL).

Immunohistochemical Analyses

Immunohistochemical analysis was performed on frozen sections as described.[16] Sections were incubated with anti-σR1 antibody[9] (1:400), followed by incubation with AlexaFluor-555-conjugated donkey anti-rabbit IgG secondary antibody (1:1000). Slides were incubated with Hoechst stain, coverslipped, and viewed with an epifluorescence microscope (Axioplan-2; Carl Zeiss Meditec, Oberkochen, Germany, equipped with the AxioVision program, ver. 4.6.3 and an HRm cam-

TABLE 1. Summary of Mice Used in the Analyses

Mouse Genotype	*n*	Age (wk)	Body Weight (g)*
RT-PCR, qRt-PCR, and Western Blot Analysis to Examine σR1 Gene/Protein Expression in Retina			
$\sigma R1^{+/+}$ (wild type)	8	5–6	18.2 ± 0.3
$\sigma R1^{+/-}$ (heterozygous)	4	5–6	17.8 ± 0.2
$\sigma R1^{-/-}$ (homozygous, knockout)	8	5–6	17.2 ± 0.3
$\sigma R1^{+/+}$ (wild type)	3	18	31.5 ± 1.0
$\sigma R1^{+/-}$ (heterozygous)	3	18	30.8 ± 1.0
$\sigma R1^{-/-}$ (homozygous, knockout)	3	18	31.3 ± 1.5
Immunohistochemistry to Examine σR1 Protein Expression in Retina and TUNEL Assay			
$\sigma R1^{+/+}$ (wild type)	3	5–6	17.3 ± 2.0
$\sigma R1^{+/-}$ (heterozygous)	3	5–6	17.6 ± 0.6
$\sigma R1^{-/-}$ (homozygous, knockout)	3	5–6	17.4 ± 1.2
$\sigma R1^{+/+}$ (wild type)	3	18	29.3 ± 1.6
$\sigma R1^{+/-}$ (heterozygous)	3	18	28.2 ± 1.6
$\sigma R1^{-/-}$ (homozygous, knockout)	3	18	28.6 ± 1.3
ERG Analysis of Retinal Function and Subsequent Light Microscopic/Morphometric Analysis (5 and 18 wk)			
$\sigma R1^{+/+}$ (wild type)	7	5–6	18.3 ± 1.0
$\sigma R1^{+/-}$ (heterozygous)	8	5–6	17.4 ± 0.5
$\sigma R1^{-/-}$ (homozygous, knockout)	8	5–6	18.6 ± 0.8
$\sigma R1^{+/+}$ (wild type)	6	18	28.9 ± 1.7
$\sigma R1^{+/-}$ (heterozygous)	6	18	29.8 ± 1.2
$\sigma R1^{-/-}$ (homozygous, knockout)	6	18	29.9 ± 0.9
Retinal Permeability Assays			
$\sigma R1^{+/+}$ (wild type)	4	18	29.1 ± 1.9
$\sigma R1^{-/-}$ (homozygous, knockout)	2	18	26.2 ± 2.7
$\sigma R1^{-/-}$ (homozygous, knockout)	2	9	27.1 ± 1.1
Ultrastructural Analysis of Optic Nerve			
$\sigma R1^{+/+}$ (wild type)	2	33	24.4 ± 1.9
$\sigma R1^{-/-}$ (homozygous, knockout)	2	33	27.8 ± 1.3
Assessment of Intraocular Pressure, ERG Analysis (59 wk), TUNEL Assay and Ultrastructure (59 wk)			
$\sigma R1^{+/+}$ (wild type)	7	18–59	23.6 ± 0.5 to 37.0 ± 1.1
$\sigma R1^{+/-}$ (heterozygous)	3	18–59	27.9 ± 2.2 to 31.5 ± 5.3
$\sigma R1^{-/-}$ (homozygous, knockout)	8	18–59	26.4 ± 1.1 to 30.5 ± 1.3

* Mean ± SEM.

era). Experiments were repeated in duplicate. Additional immunohistochemical studies were performed at 59 weeks in eyes of $\sigma R1^{+/+}$ and $\sigma R1^{-/-}$ mice using a mouse monoclonal antibody against neurofilament-light (NF-L) (1:250; Millipore, Bedford, MA) or a rabbit polyclonal antibody against cleaved caspase-3 (1:500; Cell Signaling Technology, Beverly, MA) followed by incubation with appropriate secondary antibodies. Signal intensities were quantified with image-analysis software (Metamorph, ver. 6.3; Molecular Devices, Sunnyvale, CA).

Measurement of Intraocular Pressure

The mice were anesthetized by brief (<10 seconds) exposure to isoflurane (Butler Animal Health Supply, Dublin, OH). IOP was measured at the center of the cornea using a handheld tonometer (Tonolab, Icare Laboratory; Finland Oy, Espoo, Finland). IOP was determined bilaterally in $\sigma R1^{+/+}$, $\sigma R1^{+/-}$, and $\sigma R1^{-/-}$ mice at ages 18 to 59 weeks.

Assessment of Retinal Vascular Permeability

Mice were anesthetized by intraperitoneal injection of ketamine-xylazine solution (80:12 mg/kg), perfused through the left cardiac ventricle using l mL fixative solution (4% paraformaldehyde in 0.1 M phosphate buffer, pH 7.4) containing 50 mg 20-kDa fluorescein isothiocyanate (FITC)–labeled dextran (Sigma-Aldrich, St. Louis, MO). Eyes were fixed 1 hour at 22°C; retinas were teased free from the sclera/RPE eyecup, incised at four sites and placed on microscope slides photoreceptor side facing down. Flat-mounted retinas were viewed by epifluorescence, to detect FITC-labeled dextran, and images were captured (AxioVision; Carl Zeiss Meditec).

Electrophysiological Studies

Mice, dark adapted overnight, were anesthetized as described for permeability studies. Proparacaine (0.5%) drops were applied to both eyes and pupils dilated with 1% tropicamide and 2.5% phenylephrine hydrochloride. Animals were placed on a heating pad controlled by a rectal thermometer, DTL electrodes were placed on the corneas and needle electrodes in the cheeks (references) and tail (ground). Experiments with 5- and 18-week-old animals used a series of full-field light flashes presented in a Ganzfeld (LKC, Gaithersburg, MD). Flashes were presented from dim to bright with the interstimulus interval increasing with brightness. After dark-adapted testing, animals were light-adapted for 10 minutes with a background light in the Ganzfeld (30 cd/m^2). To record cone-isolated responses, a series of full-field flashes with increasing intensity were presented in the presence of the background light. For 59-week-old mice, stimuli were generated by a custom LED-based system. A 5500° white LED was used for bright stimuli and a 470-nm blue LED for dim stimuli. The light from the blue LED was passed through neutral-density filters and defocused before collection by the optical fiber launcher to further diminish the light intensity. LED flashes of 5-ms duration were used. After the recordings, the mice were killed by CO_2 asphyxiation, and the eyes were taken for histologic processing and morphometric evaluation.

Microscopic Evaluation and Measurement Procedures

Morphometric studies were performed at 5, 18, and 59 weeks. Mice were euthanized by CO_2 asphyxiation, followed by cervical dislocation. Left and right eyes were flash frozen in OCT (Tissue-Tek; Miles Laboratories, Elkhart, IN) by immersion in liquid nitrogen. Cryostat sections (10 μm) were stained with hematoxylin and eosin. In additional studies, eyes were fixed in 2% paraformaldehyde/2% glutaraldehyde in 0.1 M cacodylate buffer and prepared for embedding (JB-4 solution; Electron Microscopy Sciences [EMS], Hatfield, PA). Microscopic evaluation of eyes included scanning tissue sections (at least three sections per eye per mouse) for evidence of gross pathology in the cornea, ciliary body/iris, lens, retina, and optic nerve. The evaluation of the lens included examining the equatorial region for pigment deposition. Subsequently, systematic morphometric analyses were performed, which included measurements of corneal thickness (from endothelium to the epithelial surface) and lens diameter at the equator. For the retina, measurements included: height of the RPE cell layer, number of cell rows in the INL and outer nuclear layer (ONL), thickness of these layers, thickness of inner and outer plexiform layers (IPL and OPL), thickness of inner and outer segments of photoreceptor cells (IS and OS), and number of cells in the GCL (expressed as cells per 100-μm retinal length). For each mouse, three sections (per eye) were analyzed. Measurements were made in three fields nasal and three fields temporal to the optic nerve, reflecting the central, midperipheral, and peripheral retina, for a total of six fields. The initial measurements were taken ~200 μm on either side of the optic nerve. Measurements were made using image analysis software (AxioVision; Carl Zeiss Meditec); data were deposited into a spreadsheet for statistical analysis.

For ultrastructural studies, $\sigma R1^{+/+}$ and $\sigma R1^{-/-}$ mice (age 33 and 59 weeks) were deeply anesthetized and perfused through the left cardiac ventricle with 2% paraformaldehyde/2% glutaraldehyde in 0.1 M cacodylate buffer. Eyes were enucleated, immersed in fixative, and postfixed with osmium tetroxide. Tissue was processed and embedded (EMbed-812; EMS). Thin sections were cut with a diamond knife on an ultramicrotome (EM UC6; Leica Microsystems, Inc., Bannockburn, IL) and collected on nickel grids. Eyes were examined with a transmission electron microscope (JEM 1230; JEOL USA. Inc., Peabody, MA) at 110 kV and imaged with a CCD camera and digital camera controller (UltraScan 4000/First Light; Gatan, Inc., Pleasanton, CA).

Analysis of DNA Fragmentation

Eyes were harvested from $\sigma R1^{+/+}$, $\sigma R1^{+/-}$, and $\sigma R1^{-/-}$ mice (5, 18, and 59 weeks). Cryosections were prepared and subjected to TUNEL analysis to detect DNA strand breaks characteristic of apoptosis. As described elsewhere,[16,20] the assay was an apoptosis detection kit (ApopTAG Fluorescein *In Situ*; Chemicon Corp., Temecula, CA), used according to the manufacturer's protocol. Slides were counterstained with DAPI (4′,6-diamidino-2-phenylindole) to label all nuclei. Tissues were viewed by epifluorescence to detect TUNEL-positive cells in cornea, lens, ciliary body, iris, retina, and ONH.

Statistical Analysis

Data for morphometric measurements, ERG analysis and TUNEL assays were analyzed by Student's *t*-test. Two-way ANOVA was used to determine significant differences in IOP; Tukey's paired comparison test was the post hoc statistical test (Prism; GraphPad, La Jolla, CA). Significance was set at $P < 0.05$.

Results

σR1 Expression

Representative mouse genotyping data are shown in Figure 1A. Neural retina, RPE/eyecup, brain, liver, and kidney were harvested and subjected to RT-PCR to detect *σR1* expression. The $\sigma R1^{+/+}$ mice had robust *σR1* expression, the $\sigma R1^{+/-}$ mice had diminished expression, and the $\sigma R1^{-/-}$ mice had no expression of *σR1* in any tissues (Fig. 1B). Immunoblot analysis detected abundant σR1 protein (M_r ~27,000) in brain and retina of the $\sigma R1^{+/+}$ mice, reduced levels in tissues of the $\sigma R1^{+/-}$ mice, and no σR1 in the $\sigma R1^{-/-}$ mice (Fig. 1C). Immunohistochemistry detected σR1 in the $\sigma R1^{+/+}$mouse retina in GCL, IPL, OPL, photoreceptor cells, and RPE (Fig. 1D). Expression levels were diminished in $\sigma R1^{+/-}$ retina and were not detected in the $\sigma R1^{-/-}$ retina. These data confirm the absence of *σR1* gene expression in the *σR1*-knockout mice.

IOP and Vascular Permeability

Elevated IOP is a feature of certain optic neuropathies including some types of glaucoma; ligands for σR1 have been shown

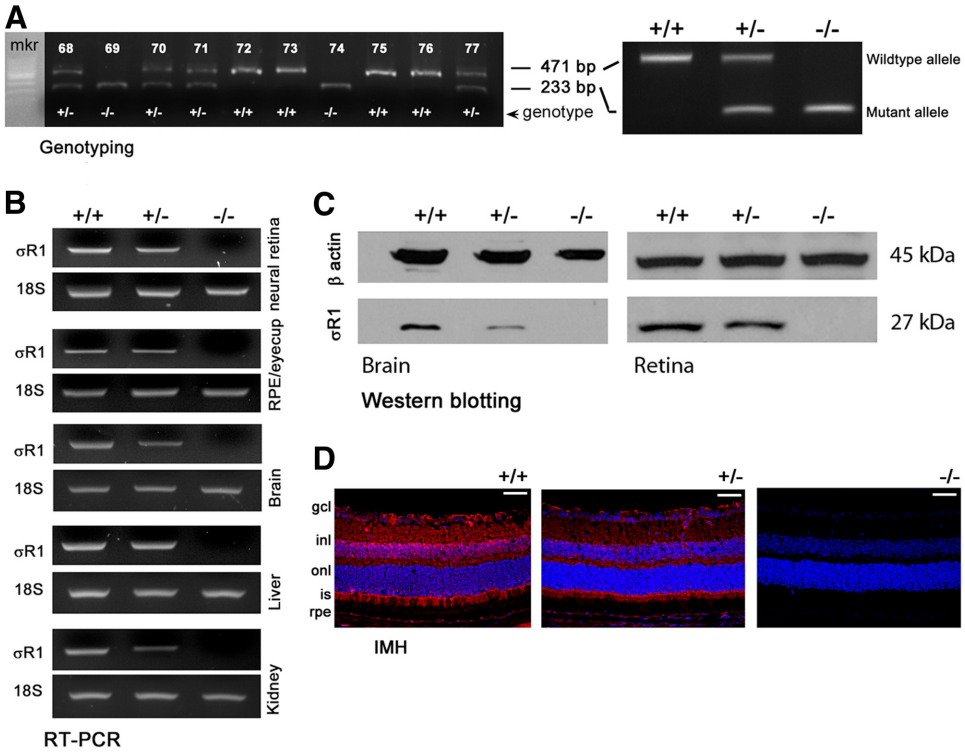

FIGURE 1. Assessment of *σR1* gene and protein expression. (**A**) Genotyping data for representative 10 offspring; mice expressing only the 471-bp product have both copies of *σR1* gene and are designated wild-type (+/+), mice expressing both the 471- and the 233-bp products have one copy of *σR1* (heterozygous, +/−), and mice expressing only the 233-bp product do not express *σR1* (homozygous, −/−). (**B**) Total RNA was isolated from neural retina, RPE/eyecup, brain, liver, and kidney and used for semiquantitative RT-PCR. Primer pairs specific for mouse *σR1* mRNA were used; *18S* RNA was analyzed in the same RNA samples as the internal control. RT-PCR products were run on a gel and stained with ethidium bromide. (**C**) Protein was extracted from brain and retina and subjected to SDS-PAGE, followed by immunoblotting first with an affinity-purified antibody against σR1 and subsequently with an antibody against β-actin (internal loading control). The 27-kDa band represents σR1, and the 45-kDa band represents β-actin. (**D**) Cryosections of mouse eyes from $\sigma R1^{+/+}$, $\sigma R1^{+/-}$, and $\sigma R1^{-/-}$ mice that were incubated with an antibody against σR1 followed by incubation with AlexaFluor 555 (*red*)-labeled secondary antibody. Scale bar, 50 μm.

to have pressure-reducing properties in the rabbit model.[21] To determine whether the absence of σR1 is associated with altered pressure, IOP was determined in the $\sigma R1^{+/+}$, $\sigma R1^{+/-}$, and $\sigma R1^{-/-}$ mice using a tonometer designed for IOP measurements in rodent eyes. The IOP of the $\sigma R1^{+/+}$ mice was ~12 to 14 mm Hg over the age range studied (18–59 weeks). In mice lacking one (+/−) or both (−/−) copies of the *σR1* gene, the IOP measurements were similar to those in the $\sigma R1^{+/+}$ mice (Fig. 2A), suggesting no direct role of σR1 in mediating IOP.

The central retinal vessels ramify within the retinal nerve fiber layer; in certain disease conditions, ischemia and/or vascular tortuosity may be associated with atrophy of the optic nerve, limiting blood to various regions. To determine whether $\sigma R1^{-/-}$ mice demonstrate alterations in retinal vascular permeability, the pattern of vascular filling of FITC-labeled dextran was examined in retinal whole mounts. Retinas in which the vasculature is intact sequester dextran within the vessels, which appear as distinct tubular structures by epifluorescence. Leaky vessels do not restrict the fluorescently labeled dextran, resulting in a diffuse pattern of fluorescence, and ischemia is reflected in vessels that fail to fill with blood. Low-magnification examination of whole mount retinas of the $\sigma R1^{+/+}$ mice showed appropriate filling of retinal vessels and no leakage of blood or ischemic regions (Fig. 2B). Higher-power examination (Fig. 2C) showed that the fluorescence is confined to the tubular structures; nonvascular regions do not fluoresce. These data are consistent with appropriate vascularization patterns. Similar data were obtained when retinal whole mounts of the $\sigma R1^{-/-}$ mice were examined (Figs. 2D, 2E). These data suggest that retinal vascularization is not altered by lack of σR1.

Electrophysiological Analysis

Comprehensive electrophysiological visual function testing was performed for the $\sigma R1^{+/+}$, $\sigma R1^{+/-}$, and $\sigma R1^{-/-}$ mice at postnatal weeks 5, 18, and 59 (only the $\sigma R1^{+/+}$ and $\sigma R1^{-/-}$ mice were tested in the 59-week-old group). At 5 and 18 weeks, a-wave amplitudes and slopes for the $\sigma R1^{+/+}$, $\sigma R1^{+/-}$, and $\sigma R1^{-/-}$ mice were identical. Statistical analyses of a-wave amplitudes, implicit times, and b-wave amplitudes showed no difference across groups at 5 or 18 weeks. Oscillatory potentials were normal at these ages. Thus, mice lacking σR1 do not manifest any alterations of the full-field ERG through at least 5 months (data not shown).

When mice were evaluated at 59 weeks, there were alterations in the b-wave amplitudes of the $\sigma R1^{-/-}$ mice (Fig. 3). Figure 3A illustrates averaged scotopic responses of 1-year-old $\sigma R1^{+/+}$ and $\sigma R1^{-/-}$ mice at a range of bright 5-ms flash intensities, expressed in log scotopic troland-seconds. Amplitudes of a-, b-, and c-waves are compared in Figures 3B–D. Although the $\sigma R1^{-/-}$ mice had slightly smaller a-waves than

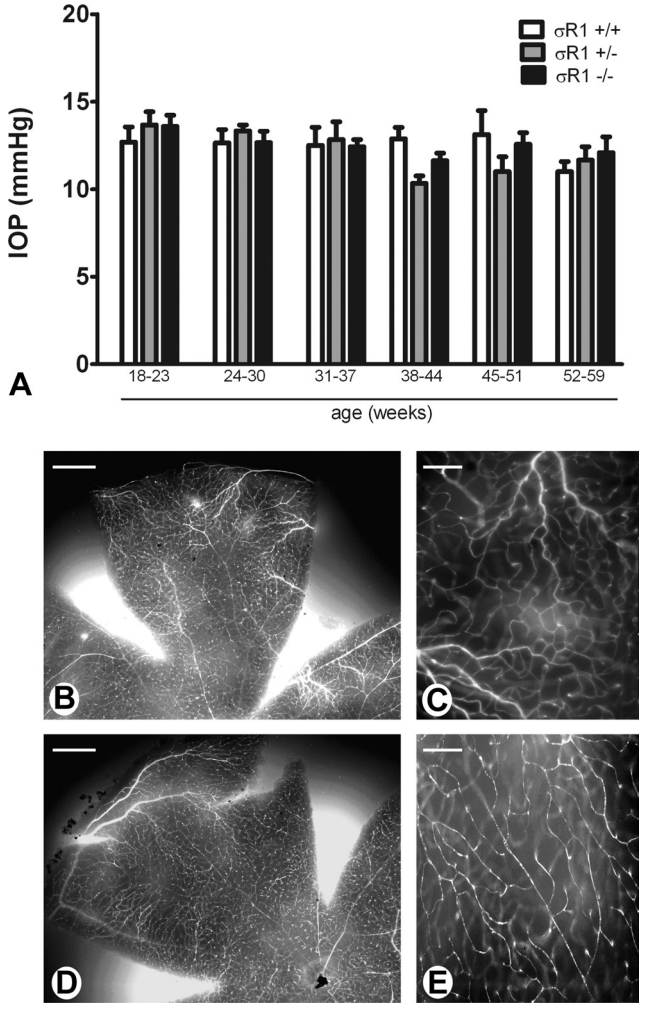

FIGURE 2. Assessment of intraocular pressure and retinal vascular permeability. (**A**) Intraocular pressure was measured by tonometry in $\sigma R1^{+/+}$, $\sigma R1^{+/-}$, and $\sigma R1^{-/-}$ mice, beginning at postnatal age 18 weeks. Measurements continued through postnatal age 59 weeks. Data represent the mean ± SEM for both eyes of at least three mice per group. There were no statistically significant differences in IOP among the three groups of mice over the ages examined. (**B**–**E**) $\sigma R1^{+/+}$ (**B**, **C**) and $\sigma R1^{-/-}$ (**D**, **E**) mice were perfused through the left cardiac ventricle with FITC-labeled dextran, to visualize vessels in retinal whole mounts. Low-magnification (**B**, **D**) images of whole mount retinas reveal filling of retinal vessels (bright fluorescence), which was better visualized at higher magnification (**C**, **E**). Data are representative images of the eight mice analyzed in the study. Scale bar: (**B**, **D**) 200 μm; (**C**, **E**) 50 μm.

did the $\sigma R1^{+/+}$ mice (Fig. 3B), much more striking differences were observed in b-wave amplitudes of the $\sigma R1^{-/-}$mice, which were significantly smaller than the $\sigma R1^{+/+}$ at all intensities (Fig. 3C). The c-wave amplitudes were similar across mice (Fig. 3D). The c-wave is a late positive response, generated largely from the RPE (shown in the inset) that includes the full time course of the response at −0.4 log scotopic troland-seconds.

One-year-old mice were tested for scotopic threshold responses (STRs; Fig. 4). These are the most sensitive ERG responses one can observe with dim stimuli in the dark-adapted state.[22,23] They were obtained with 5-ms flashes of a blue (470 nm) LED, made dimmer with neutral-density filters and defocusing. Just above threshold, a late negative potential develops at ~200 ms after the flash; this is the negative (n)STR. At slightly higher intensities, a positive potential emerges at approximately 110 ms, the positive (p)STR. The inset in Figure 4A shows an example of the ERG signals in $\sigma R1^{+/+}$ and $\sigma R1^{-/-}$ mice and how these amplitudes are measured. The pSTR eventually merges into the b-wave at higher intensities, and the nSTR is submerged by these long-lasting positive potentials. The STRs in mice are generated in large part by RGCs[23] and serve as a measure of RGC function. The 1-year-old $\sigma R1^{-/-}$ mice had diminished nSTRs than did the $\sigma R1^{+/+}$ mice (Fig. 4A); the pSTRs were slightly weaker as well, but the differences were not significant (Fig. 4B).

Microscopic and Morphometric Analysis

Systematic evaluation of eyes of the $\sigma R1^{+/+}$, $\sigma R1^{+/-}$, and $\sigma R1^{-/-}$ mice included analysis of the anterior and posterior regions of the eye. Corneas of $\sigma R1^{+/+}$, $\sigma R1^{+/-}$, and $\sigma R1^{-/-}$ mice appeared intact and were of comparable thickness (120.9 μm +/− 5.3 vs. 113.8 μm +/− 4.0 for the $\sigma R1^{+/+}$ and $\sigma R1^{-/-}$ mice, respectively). The ciliary body and iris showed no gross pathology in any of the groups of mice examined. There was no evidence of anterior or posterior synechiae, which are respectively attachments of the iris to the cornea anteriorly or the lens posteriorly. The iridial pigment epithelium appeared similar in thickness and pigment distribution in $\sigma R1^{-/-}$ mice compared with wild-type. There were no differences in lens epithelial cells among the three mouse groups. Representative photomicrographs of ciliary body/iris/cornea (Figs. 5A, 5B), higher magnification of cornea (Figs. 5C, 5D), lens (Figs. 5E, 5F), and retina (Figs. 5G, 5H) are shown in Figure 5.

In vitro studies of Wang et al.[7] showed that when lens capsular cells are cultured in the presence of BD1047, a σR1 antagonist, pigment granules are observed by transmission electron microscopy (TEM), and their formation appears to follow the developmental stages of pigmentation. We asked whether absence of σR1 in vivo leads to lens pigmentation. Using TEM, we examined lenses in mice (ages 18, 33, and 59 weeks), but did not observe pigment deposition nor the developmental stages described for pigment formation.[24] Lens morphology in the $\sigma R1^{-/-}$ mice was similar to that in the $\sigma R1^{+/+}$ mice (Fig. 6).

Light microscopic examination of the retina showed no gross pathology in the $\sigma R1^{-/-}$ mice at 5 (data not shown) or 18 (Fig. 5H) weeks. Comprehensive morphometric analysis of retinal thickness; thickness of INL, ONL, IPL, OPL; number of rows of cells in the INL and ONL; and numbers of cells in the GCL did not reveal statistically significant differences at 5 or 18 weeks in the $\sigma R1^{+/-}$ and $\sigma R1^{-/-}$ mice compared to the $\sigma R1^{+/+}$ mice (data not shown). TUNEL analysis revealed no evidence of dying cells in retina, cornea, or other ocular tissues (data not shown). There were, however, TUNEL-positive cells detected in the ONH of the $\sigma R1^{-/-}$ mice at 18 weeks (Fig. 7B), which was not the case in the wild-type mice (Fig. 7A). At 1 year, significantly more TUNEL-positive cells were apparent in this region in the $\sigma R1^{-/-}$ mice (Fig. 7C) compared to the control mice (quantitative data presented in Fig. 7D).

Ultrastructural Analysis of the ONH and GCL and Morphometric Analysis at Older Ages

The presence of TUNEL-positive cells at 18 weeks prompted ultrastructural inspection of ONH and GCL in $\sigma R1^{-/-}$ mice at older ages (33 weeks). Although early studies suggested that mice lack a lamina cribrosa,[25] more recent data suggest that they have a glial lamina[26]; thus, we used this terminology in describing the data. Figures 8A–C are light micrographs of the ocular region examined at the ultrastructural level. Figures 8D–F indicate the distinction between the prelaminar and laminar regions of the ONH. The axons, glial columns, and astrocytes are visible in the prelaminar (Figs. 8G–L) and laminar

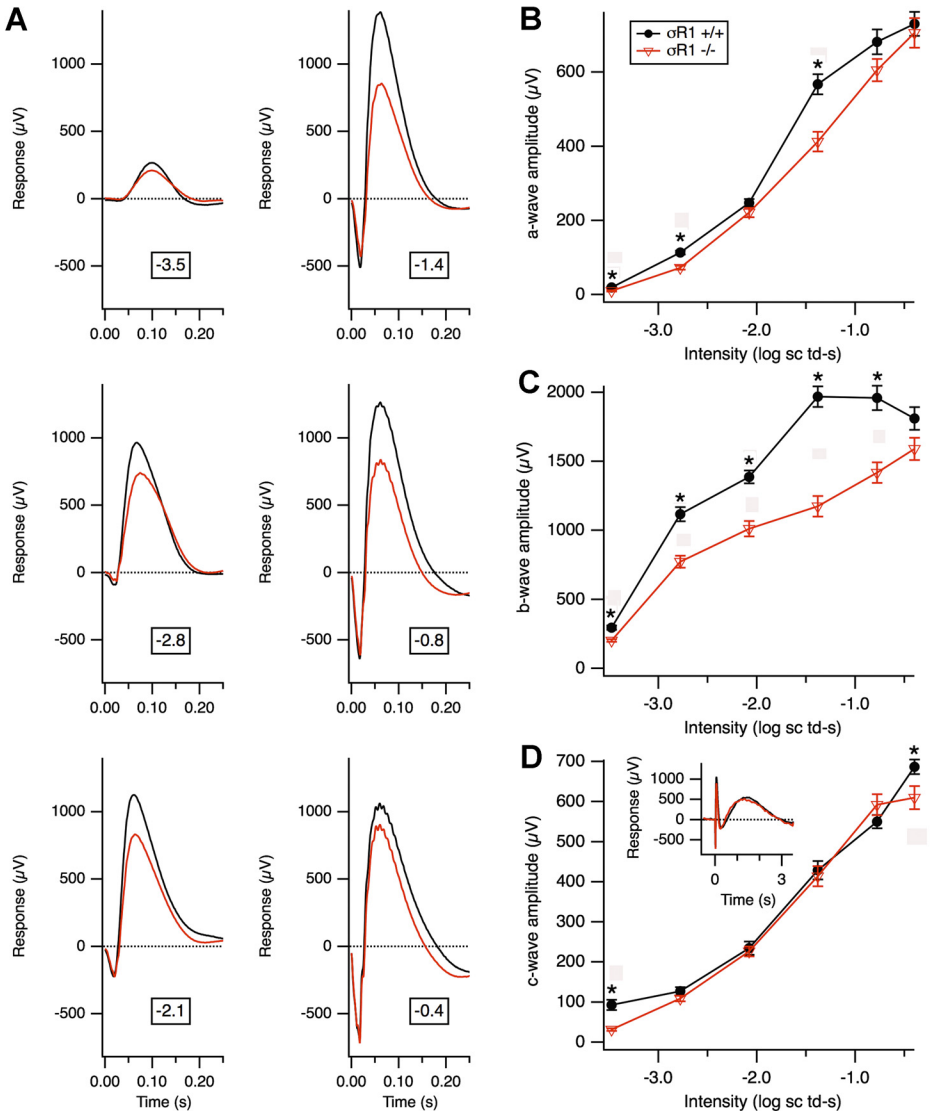

Figure 3. Electrophysiological assessment of retinal function in 1-year-old $\sigma R1^{-/-}$ mice. (**A**) Electrophysiological visual function analysis performed under scotopic conditions over a range of bright flash intensities (expressed as log scotopic troland-seconds) in $\sigma R1^{+/+}$ ($n = 4$) and $\sigma R1^{-/-}$ ($n = 5$) mice at age 59 weeks. Data represent averaged values for the mice in the two groups. Graphic depiction of the average (**B**) a-, (**C**) b-, and (**D**) c-wave amplitudes in $\sigma R1^{+/+}$ compared with $\sigma R1^{-/-}$ mice. (**D**, *inset*) The full time course of the response at −0.4 log scotopic troland-seconds; the c-wave is the late positive response. *Significantly different from $\sigma R1^{-/-}$ mice; $P < 0.05$.

(Figs. 8M–O) areas of the optic nerve. In $\sigma R1^{+/+}$ mice, ONH axons are uniform in size with an occasional glial column or astrocytes in proximity to many axonal processes. The mitochondria are easily visible organelles distinguished by their abundant cristae. The mitochondria in $\sigma R1^{+/+}$ mice were of uniform size. In contrast, the ONH of the $\sigma R1^{-/-}$ mice had swollen axons, particularly in the laminar regions (Figs. 8N, 8O). There were dystrophic neurites in which swollen and damaged axon segments containing an accumulation of organelles (such as swollen mitochondria) were evident (Figs. 8H, 8I). Dying cells were evident in the prelaminar region of the $\sigma R1^{-/-}$ mice (Figs. 8K, 8L). Their nuclei were more lightly stained than those of healthy cells and there was a decrease in the cytoplasm. In Figure 8L, the apoptotic cell is surrounded by a phagocytic cell. Within the ONH region, there are ganglion cell axons and cell bodies of astrocytes and oligodendrocytes, although the specific type of glial cell undergoing apoptosis is not certain.

Since axons were disrupted in the ONH of the older $\sigma R1^{-/-}$ mice, we asked whether there was evidence of apoptosis in the RGCs, the source of these axons, in the σR1-null mice. Ultrastructural examination of the GCL showed that the $\sigma R1^{+/+}$ mice (age 59 weeks) had normal-appearing neurons; cell bodies were plump, and there was no evidence of apoptotic cell death (Figs. 9A, 9C) consistent with the TUNEL assay data described above (Figs. 7A, 7D). Retinas of the age-matched $\sigma R1^{-/-}$ mice showed cell dropout and apoptosis in the GCL (Figs. 9B, 9D). These data were confirmed by immunohistochemical detection of active caspase-3 in the GCL of the 1-year-old $\sigma R1^{-/-}$ mice (Fig. 9H), which was not detected in the age-matched $\sigma R1^{+/+}$ mice (Fig. 9F). Quantification of the number of cells in the GCL revealed significantly fewer cells (expressed per 100-μm length of retina) in the $\sigma R1^{-/-}$ mice than in the $\sigma R1^{+/+}$ (Fig. 9I), particularly in the central retina. In the peripheral retina, there were fewer cells in the GCL in the $\sigma R1^{-/-}$ mice than in the $\sigma R1^{+/+}$ mice, but the data did not reach statistical significance. Although significant differences were observed in the number of cells in the GCL between the $\sigma R1^{-/-}$ and $\sigma R1^{+/+}$ mice, systematic morphometric analysis of the other nuclear and synaptic layers did not reveal significant differences between the two mouse groups (data not shown). In the retinas, only the RGCs were consistently labeled with antibodies directed against neurofilament proteins (NF); the three NF proteins light (NF-L, 68 kDa), medium (NF-M, 160 kDa), and heavy (NF-H, 200 kDa) are expressed in mature ganglion cells.[27] We performed immunohistochemical analysis using an antibody against NF-L to label RGC bodies and their axons and quantified the expression levels with image-analysis software (Metamorph; Molecular Devices). There was decreased expression of NF-L in retinas of the $\sigma R1^{-/-}$ mice

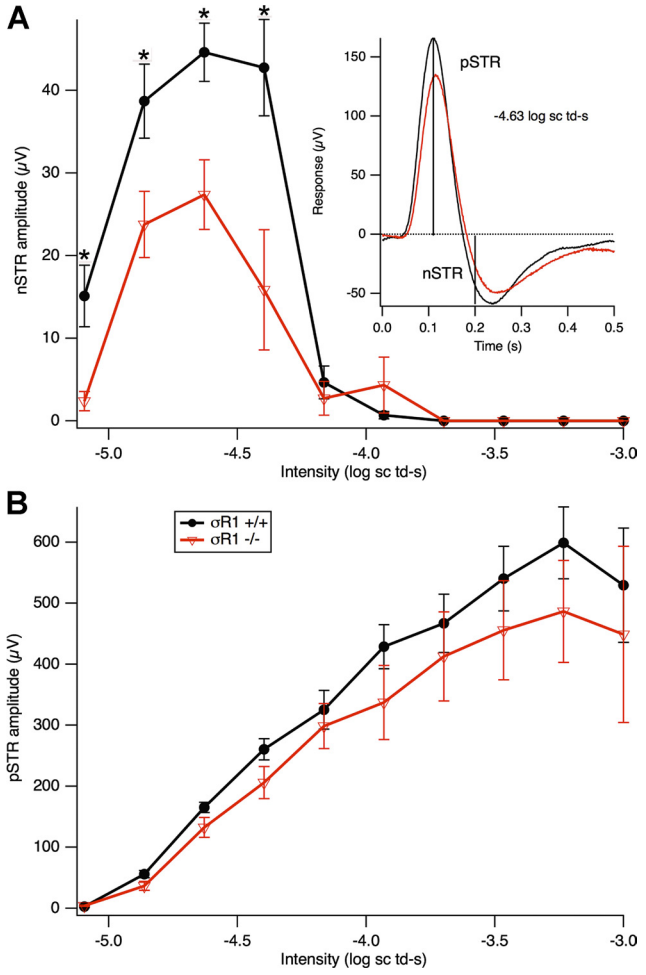

Figure 4. Scotopic threshold responses in 1-year-old $\sigma R1^{-/-}$ mice. Electrophysiological analysis was performed under scotopic conditions over a range of dim flash intensities in $\sigma R1^{+/+}$ ($n = 3$) and $\sigma R1^{-/-}$ ($n = 3$) mice at age 59 weeks. Data represent averaged values for the mice in the two groups. (**A**) Negative and (**B**) positive scotopic threshold response (nSTR and pSTR) amplitudes are shown for $\sigma R1^{+/+}$ compared with $\sigma R1^{-/-}$ mice. (**A**, *inset*) The responses at −4.6 log scotopic troland-seconds, with vertical lines at 200 and 110 ms indicating where nSTR and pSTR amplitudes were measured. If the response at 200 ms was positive, the nSTR amplitude was set to 0. *Significantly different from $\sigma R1^{-/-}$ mice; $P < 0.05$.

(Fig. 9G), especially in the central retina, compared with the $\sigma R1^{+/+}$ mice (Fig. 9E). Taken collectively, the data shown in Figures 7, 8, and 9 suggest that with age, the retinas of mice lacking σR1 manifest disruption of RGCs and their axons.

Discussion

σR1 has been implicated in drug and alcohol addiction, amnesia, pain, depression, Alzheimer's disease, stroke, cancer, and retinal neuroprotection.[28] Whether σR1 has a direct role in these conditions is less certain. The availability of genetically manipulated mice lacking *σR1* has provided a powerful tool to clarify the role of σR1 in disease. The first study describing the *σR1* knockout mouse reported that they were viable, fertile, and did not display an overt phenotype aside from a hypermotility response on challenge with the σR1 ligand SKF-10047.[29] Data obtained from subsequent analyses of $\sigma R1^{-/-}$ mice suggest a pain-related role for σR1. Formalin-induced pain responses are reduced in $\sigma R1^{-/-}$ mice[30]; σR1 is essential for capsaicin-induced mechanical hypersensitivity, but not mechanical nociceptive pain.[31] Cold and mechanical allodynia did not develop in $\sigma R1^{-/-}$ mice exposed to sciatic nerve injury.[32] Analyses of $\sigma R1^{-/-}$ mice have shown that σR1 has a role in modulation of depressive-like behavior assessed in forced swimming tests,[19] in elimination of the *N*,*N*-dimethyltryptamine (DMT)-induced hypermobility response,[33] in regulation of motor behavior,[34] and in decreased modulation of Na^+-currents in cardiac myocytes.[35]

The neuroprotection conferred by σR1 ligands (+)-PTZ and SKF-10047 in RGCs in vitro[15,17] and (+)-PTZ in vivo in retinas of $Ins2^{Akita/+}$ diabetic mice,[16] coupled with the role of σR1 as a molecular chaperone interacting with BiP/GRP78,[1] led us to hypothesize that lack of σR1 protein could have a profound impact on ocular/retinal structure and function. The current studies provide comprehensive analyses of the ocular phenotype of mice lacking *σR1*.

The most profound alterations in eyes of $\sigma R1^{-/-}$ mice were observed in the retina. Whereas the initial ERG recordings of young $\sigma R1^{-/-}$ mice (through ~5 months) were within normal limits, ERG recordings of older mice (12 months) demonstrated a marked decrease in b-wave amplitude and nSTR. The b-wave is generated largely by bipolar cells; however, Müller

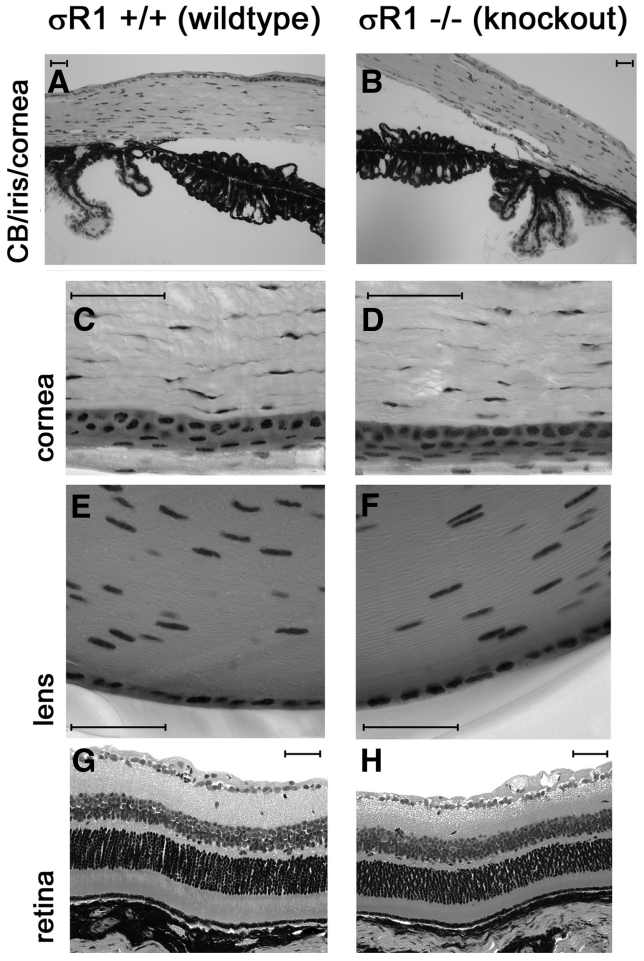

Figure 5. Light photomicrographs of eyes of wild-type and $\sigma R1^{-/-}$ mice. Eyes of wild-type (**A**, **C**, **E**, **G**) and $\sigma R1^{-/-}$ (**B**, **D**, **F**, **H**) (18 weeks) mice were fixed and embedded, and sections were cut at 2-μm thickness and viewed by light microscopy. Systematic examination of the eyes included examination of the cornea, ciliary body, and iris; the cornea (at higher magnification); the equatorial region of the lens; and the retina. Data are representative images from six to eight mice per group. Scale bar, 50 μm.

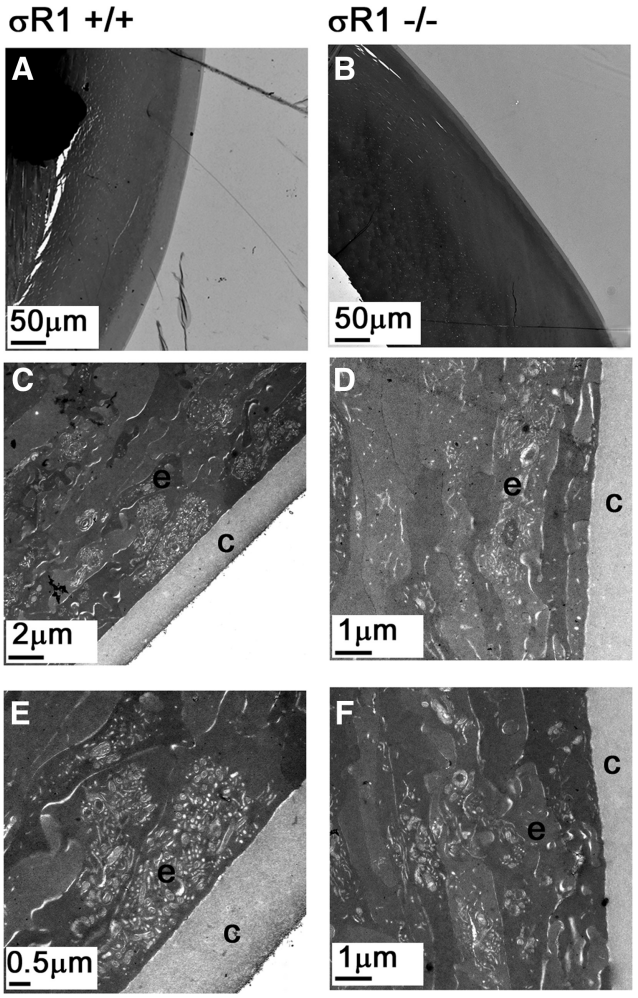

FIGURE 6. Ultrastructural assessment of the lens. Wild-type mice (**A**, **C**, **E**) and $\sigma R1^{-/-}$ mice (**B**, **D**, **F**) were perfused through the left cardiac ventricle, and eyes were prepared for electron microscopy. (**A**, **B**) Light photomicrograph (low magnification) depicting the equatorial region of the lens. (**C**–**F**) Electron photomicrographs of the lens showing the capsule (c) and the lens epithelial cells (e) at the equatorial region. There was no evidence of pigment granule formation in the wild-type or *σR1*-knockout mouse lens. These images are from two mice in each group at ages 33 and 59 weeks.

cells also contribute.[36] The link between b-wave amplitude and bipolar function is complex and can be affected by changes in OFF-bipolar, Müller, amacrine, and ganglion cells. In the mouse, σR1 expression has been reported in Müller[11] and ganglion cells[2,9,10,11,13,15] as well as other retinal cell types.[2,11] There has been a recent report in rat retina suggesting that σR1 may not co-localize with certain bipolar cell somata[17]; however, σR1expression has not been investigated in mouse bipolar cells. Our electrophysiological analysis also revealed diminished nSTR in the $\sigma R1^{-/-}$ mice. The nSTR is a highly sensitive measure of RGC function, and it may reflect reduced signaling of bipolar cells as well. The interpretation of the electrophysiological data obtained in this study is that inner retinal function, particularly of RGCs is most affected in the year-old $\sigma R1^{-/-}$ mice. The morphologic and morphometric analysis supported these observations. There were significantly fewer cells in the GCL, especially in the central retina in the 12-month-old $\sigma R1^{-/-}$ mice, than in the age-matched controls. We detected active caspase-3 in the GCL of 12-month-old mice and expression of neurofilament protein NF-L was noticeably diminished in the GCL of the *σR1*-null animals. Systematic measurements of other retinal layers, including the thickness of the INL, revealed no significant differences in the *σR1*-null mice compared with wild-type. Whether neurons in the INL or ONL die at much older ages in the $\sigma R1^{-/-}$ mice warrants further study.

Interestingly, we did not observe dying cells in the GCL in mice that were younger than 6 months; however, we did observe alterations in the ONH of the $\sigma R1^{-/-}$ mice. At 18 weeks, TUNEL-positive cells were present in the astrocyte-rich region of the ONH of the $\sigma R1^{-/-}$ mice, which forms a mesh-like network of glial cells through which RGC axons pass. The astrocytes are intimately associated with axons of the ONH.[26]

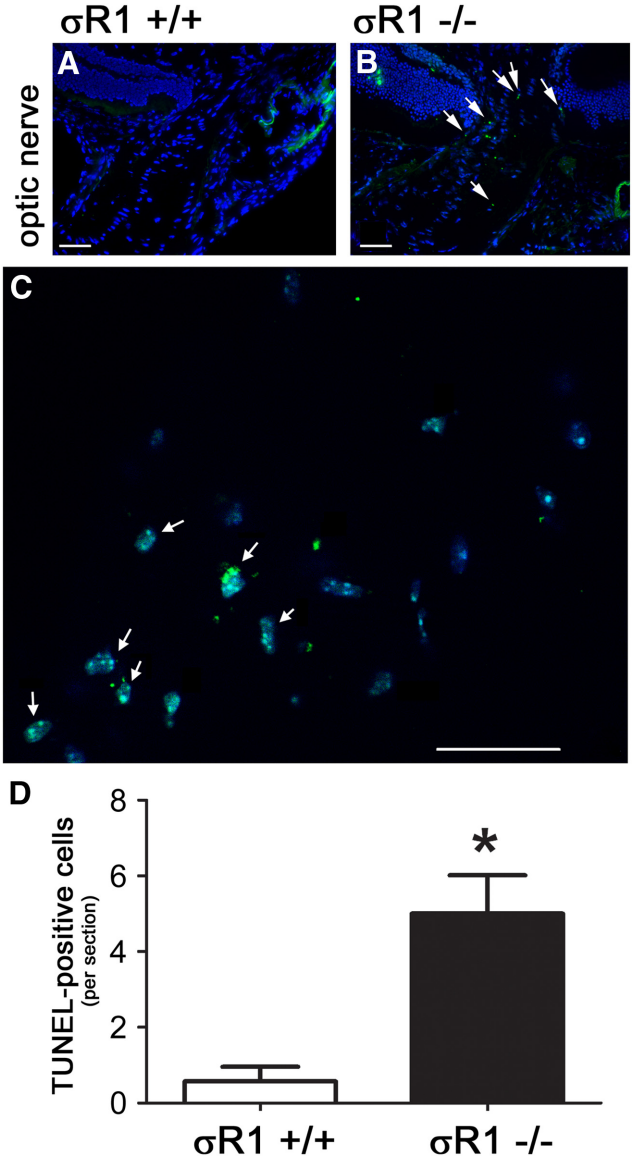

FIGURE 7. TUNEL analysis was performed on cryosections of the ONH of (**A**) $\sigma R1^{+/+}$ and (**B**) $\sigma R1^{-/-}$ mice (postnatal age, 18 weeks). Higher magnification images of TUNEL-positive cells in this region were obtained in $\sigma R1^{-/-}$ mice (postnatal age, 59 weeks). *Green* and *blue* fluorescent signals reflect TUNEL-positive and DAPI staining of nuclei, respectively. (**C**) Numerous TUNEL-positive cells were detected in the ONH of the $\sigma R1^{-/-}$ mice (*arrows*). Quantitation of the number of TUNEL-positive cells per section at 59 weeks is shown in the graph in (**D**). *Significantly different from the $\sigma R1^{+/+}$ mice $P < 0.05$; both eyes were analyzed in three mice per group, experiments were performed in triplicate.

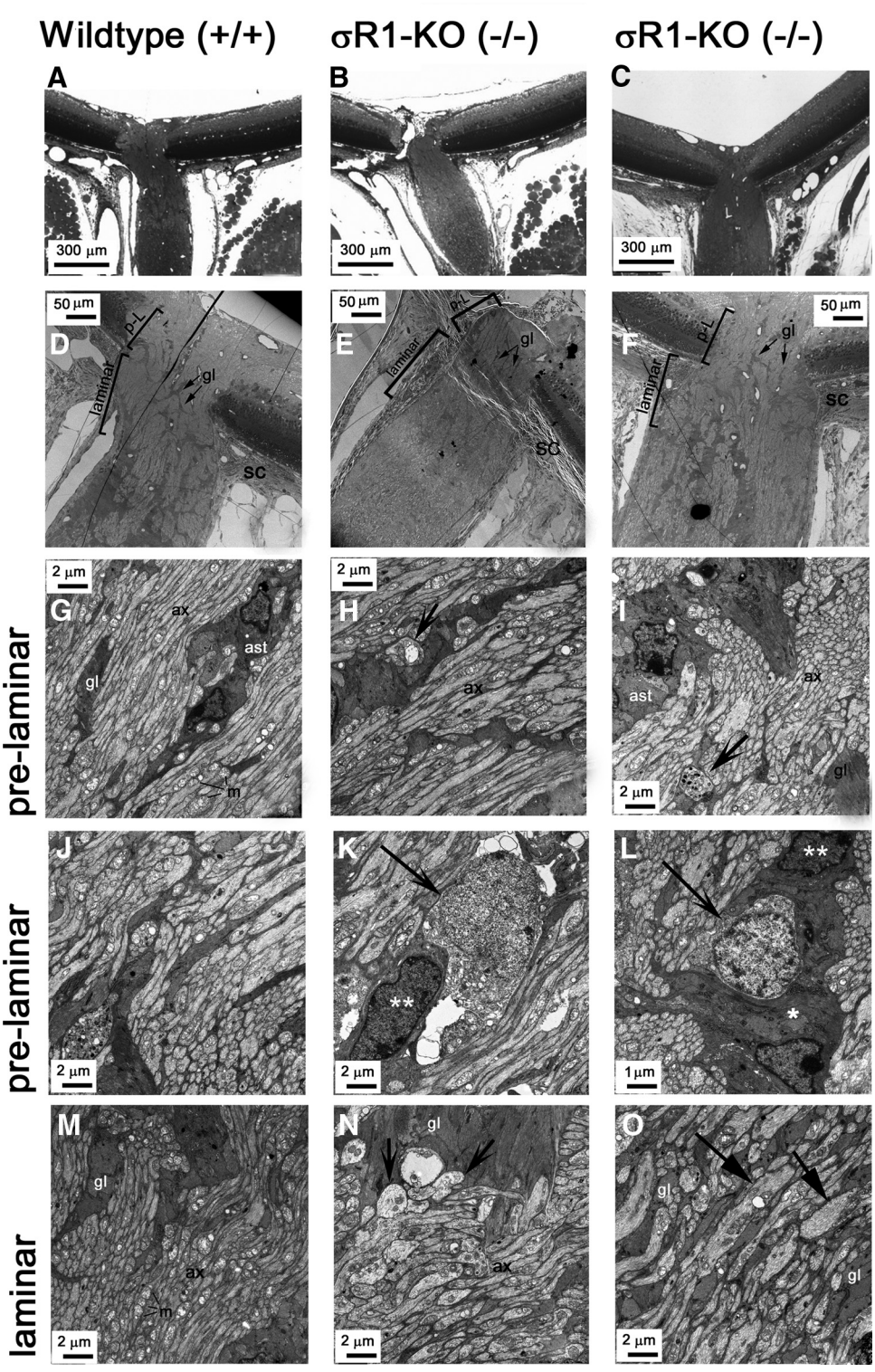

FIGURE 8. Ultrastructural assessment of the optic nerve head. Wildtype (**A**, **D**, **G**, **J**, **M**) and $\sigma R1^{-/-}$ (**B**, **C**, **E**, **F**, **H**, **I**, **K**, **L**, **N**, **O**) mice were perfused through the left cardiac ventricle, and eyes were prepared for electron microscopy. (**A–C**) Light photomicrograph (low magnification) depicting the region of the optic nerve head (ONH) examined by electron microscopy. (**D–F**) Low-magnification electron photomicrographs of the ONH showing the prelaminar (p-L) and laminar regions. High-magnification electron photomicrographs of the prelaminar (**G–L**) and laminar (**M–O**) regions of optic nerve. (**H**, **I**, **N**, *arrows*) Dystrophic neurites with accumulated organelles, especially mitochondria. (**K**, **L**, *arrows*) Apoptotic cells. (**L**) The apoptotic cell is surrounded by a phagocytic cell (*arrow*); (✱) and (✱✱) The cytoplasm and nucleus of the phagocytic cell, respectively. (**O**, *arrows*) Swollen axons surrounded by numerous glial columns. gl, glial columns; m, mitochondria; ax, axons; ast, astrocytes.

Within this glial laminar region of the optic nerve, many TUNEL-positive glial cells were detected. There have been no investigations of the role of σR1 in maintaining glial cells, but our data suggest a role for their survival as well. The TEM analysis of the ONH revealed disruption of the axonal processes. The axon fibers in the *σR1*-null mice were swollen with accumulation of various organelles, especially mitochondria. It appears that alterations of the ONH presage the retinal dysfunction and death observed in later months in the *σR1*-null mice. Regarding the optic nerve, the present work was restricted to the ONH region; however, future work in which the distal optic nerve is examined could be very informative, as distal axonopathies are observed in neurodegenerative diseases such as glaucoma.

The alterations of the ONH and subsequent RGC loss were not accompanied by an increase in IOP or a change in retinal vascularization. In all three mouse groups examined ($\sigma R1^{+/+}$, $\sigma R1^{+/-}$, and $\sigma R1^{-/-}$), the IOP was ~10 to 15 mm/Hg and held steady over the course of the 1-year period of study. Histologic assessment of the anterior eye (cornea, iris/ciliary

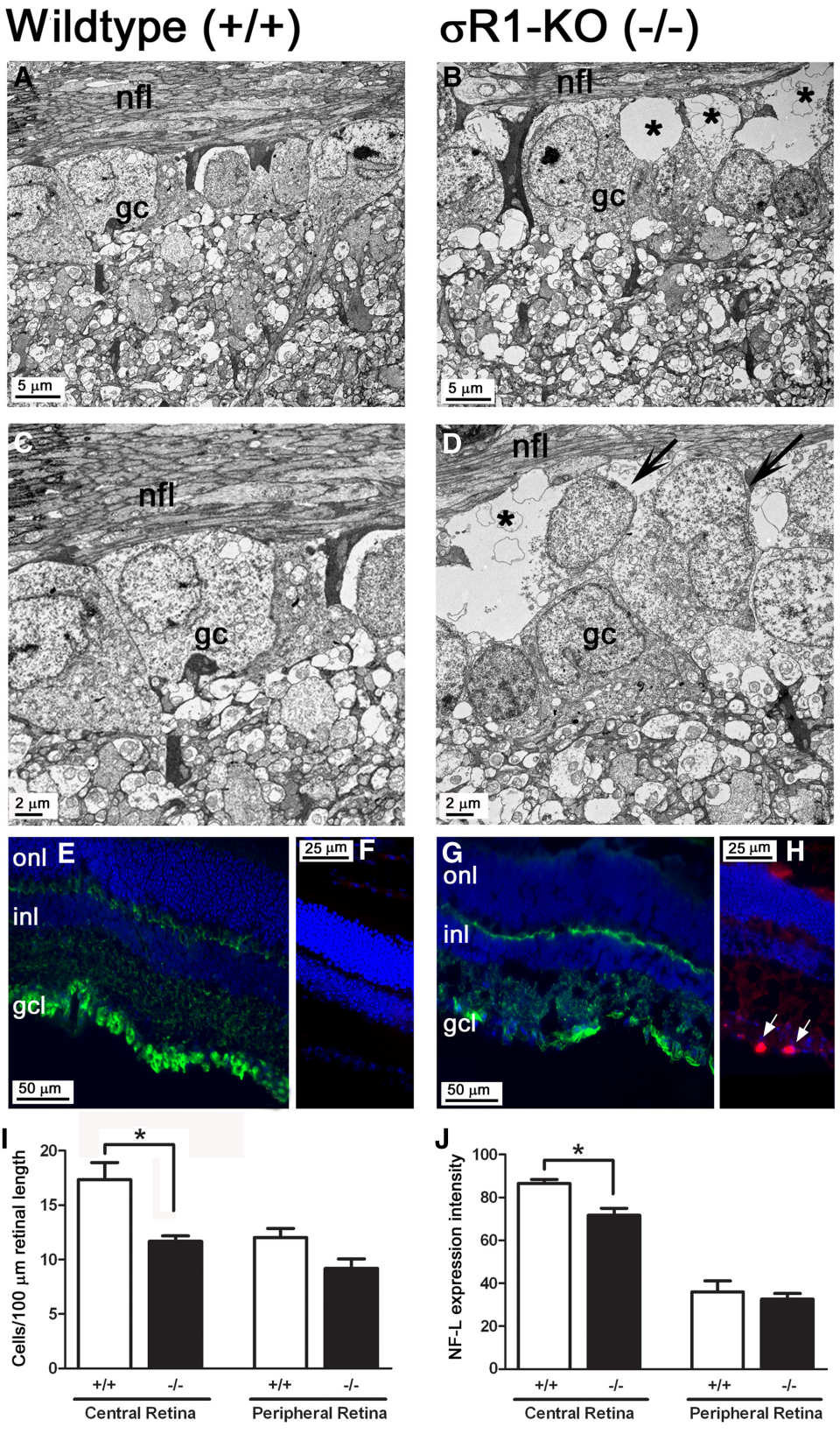

Figure 9. Ultrastructural and immunohistochemical analysis of the GCL. Mice (age 59 weeks) were perfused through the left cardiac ventricle, and eyes were prepared for TEM. (**A**) Nerve fiber layer (nfl) and GCL of $\sigma R1^{+/+}$ mice showing plump ganglion cell bodies (gc) with no evidence of apoptosis; (**C**) higher magnification of cells in (**A**). (**B**) Nerve fiber layer and ganglion cells of the $\sigma R1^{-/-}$ mice showing healthy ganglion cell (gc) adjacent to an area of cell drop out (1010). (**D**) Higher magnification of an area with two cells undergoing apoptosis (*arrowheads*) in $\sigma R1^{-/-}$ mice. Eyes were prepared for immunohistochemistry to detect neurofilament-light protein (NF-L) and active caspase-3 in $\sigma R1^{+/+}$ (**E**, **F**) and $\sigma R1^{-/-}$ mice (**G**, **H**). *Green* and *blue* fluorescent signals reflect NF-L and DAPI staining of nuclei, respectively; levels of NF-L were robust in the ganglion cells (gcl) of the $\sigma R1^{+/+}$ mice (**E**), but were diminished in $\sigma R1^{-/-}$ mice (**G**). Immunodetection of active caspase-3 (*red* fluorescence) in $\sigma R1^{+/+}$ (**F**) and $\sigma R1^{-/-}$ mice (**H**) confirmed apoptosis in the GCL (gcl) of $\sigma R1^{-/-}$ mice (*arrows*); *blue*: cell nuclei (DAPI). (**I**) Quantitative analysis of the number of cells in the GCL determined for the central and peripheral retina; *significantly different from wild-type, $P < 0.05$. (**J**) Quantitative analysis of the expression levels of NF-L; *significant difference in fluorescence intensity from wild-type; $P < 0.05$. Both eyes were analyzed in three mice per group; experiments were performed in triplicate.

body) also showed no differences between the wild-type and $\sigma R1^{-/-}$ mice, which is consistent with the normal IOP. Vascularization was also similar between the $\sigma R1^{-/-}$ and $\sigma R1^{+/+}$ mice, with no evidence of tortuous vessels, areas of ischemia, or vascular leakiness.

It is enigmatic that *σR1* has a ubiquitous ocular expression pattern, yet lack of the gene and its protein product results in an apparently discreet functional phenotype. The data obtained herein suggest that in mice lacking *σR1*, it is primarily inner retinal function and structure that are af-

fected, but it is not clear why RGCs should be more susceptible to absence of σR1 than other retinal neurons. Insights into this intriguing observation may be related to the role σR1 plays in regulating calcium signaling[17,18] and acting as a molecular chaperone.[1,13]

σR1 plays a key role in regulating intracellular calcium, and alterations in calcium homeostasis have been implicated in development of some forms of optic neuropathy.[37] Calcium ions serve as important intracellular signals for multiple cellular processes, including proliferation and differentiation, membrane trafficking, and regulation of gene expression.[38–40] Paradoxically, calcium ions can be toxic to cells and can trigger events leading to apoptosis in various cell types.[40] Thus, there must be tight regulation of calcium levels. Within cells, inositol (1,4,5)-trisphosphate receptors (IP_3Rs) mediate calcium release from intracellular calcium stores in ER. Agonists for σR1 enhance IP_3-dependent calcium release from ER by inducing dissociation of ankyrin B 220 from the IP_3R.[41] σR1 resides at the ER–mitochondrial membrane and, under cellular stress, can translocate from the mitochondria into the ER to counteract apoptosis. It is possible that absence of σR1 during long-term stress eventually leads to apoptosis of retinal neurons, particularly RGCs. The role of σR1 in regulating calcium and subsequent signaling of apoptotic events including decreasing the expression of Bax levels, as well as limiting caspase-3 activation has been demonstrated experimentally in the retinal neuronal cell line (RGC-5).[42]

Related to its role in regulating calcium via IP_3R, σR1 may also mediate ER stress. σR1 is located on the ER membrane in RGCs,[13] Müller cells,[12] and other cell types.[1] The ER serves as the entry site for proteins in the secretory pathway; proteins enter the ER lumen in an unfolded state and require protein chaperones and catalysts of protein folding to attain their final appropriate conformation. Misfolded proteins do not progress through the secretory pathway; rather, they are directed toward a degradative pathway (ERAD). Unfolded proteins are prohibited from accumulating in the ER by the intracellular signaling pathway known as the unfolded protein response (UPR). This dynamic process involves BiP/GRP78, a key regulator of ER stress. Insults such as increased intraluminal calcium, altered glycosylation, and nutrient deprivation can trigger disrupted protein folding in the ER lumen and activate the UPR. If conditions persist, apoptosis is initiated. This sequence of events plays a pivotal role in the pathogenesis of several neurodegenerative diseases.[43] We reported previously that σR1 binds BiP/GRP78. Binding increased when retinal cells were exposed to oxidative stress,[13] but decreased when cells were treated with the σR1 ligand (+)-PTZ. σR1 may modulate the function of BiP/GRP78 in such a manner as to forestall the long-term consequences of chronic ER stress.

The late-onset functional and structural dysfunction we have discovered through this comprehensive assessment of the $\sigma R1^{-/-}$ mouse retina strongly suggests that σR1 has an important role in protecting the inner retina against stress. σR1 may not be necessary for normal ocular/retinal development, but it appears to play a critical role in coping with long-term retinal cellular stress. This putative protective role is borne out by the recent discovery that mice lacking σR1 demonstrated accelerated RGC death after acute damage to the optic nerve compared with wild-type mice.[11]

In conclusion, this is the first report of the effect of the absence of σR1 on ocular function. The marked loss of inner retinal function, loss of RGCs, and disruption of the ONH suggest that studies of σR1 may prove useful in understanding mechanisms associated with some forms of optic neuropathy.

Acknowledgments

The authors thank Elizabeth Perry and Penny Roon (Medical College of Georgia Histology/Electron Microscopy Core Facility) for excellent assistance with the ultrastructural studies, Qian He for work on the initial morphometric analysis of the retinas, and Denise Zamora for the preparation of the manuscript.

References

1. Hayashi T, Su TP. Sigma-1 receptor chaperones at the ER-mitochondrion interface regulate Ca(2+) signaling and cell survival. *Cell.* 2007;131:596–610.
2. Ola MS, Moore PM, El-Sherbeny A, et al. Expression pattern of sigma receptor 1 mRNA and protein in mammalian retina. *Mol Brain Res.* 2001;95:86–95.
3. Schoenwald RD, Barfknecht CF, Xia E, Newton RE. The presence of sigma-receptors in the lacrimal gland. *J Ocul Pharmacol.* 1993; 9:125–139.
4. Bucolo C, Campana G, Di Toro R, Cacciaguerra S, Spampinato S. Sigma 1 recognition sites in rabbit iris-ciliary body: topical sigma 1-site agonists lower intraocular pressure. *J Pharmacol Exp Ther.* 1999;289:1362–1369.
5. Campana G, Bucolo C, Murari G, Spampinato S. Ocular hypotensive action of topical flunarizine in the rabbit: role of sigma 1 recognition sites. *J Pharmacol Exp Ther.* 2002;303:1086–1094.
6. Wang L, Duncan G. Silencing of sigma-1 receptor induces cell death in human lens cells. *Exp Cell Res.* 2006;312:1439–1446.
7. Wang L, Prescott AR, Spruce BA, Sanderson J, Duncan G. Sigma receptor antagonists inhibit human lens cell growth and induce pigmentation. *Invest Ophthalmol Vis Sci.* 2005;46:1403–1408.
8. Senda T, Matsuno K, Mita S. The presence of sigma receptor subtypes in bovine retinal membranes. *Exp Eye Res.* 1997;64:857–860.
9. Ola MS, Moore P, Maddox D, et al. Analysis of sigma receptor (σR1) expression in retinal ganglion cells cultured under hyperglycemic conditions and in diabetic mice. *Mol Brain Res.* 2002; 107:97–107.
10. Liu LL, Wang L, Zhong YM, Yang XL. Expression of sigma receptor 1 mRNA and protein in rat retina. *Neuroscience.* 2010;167:1151–1159.
11. Mavlyutov TA, Nickells RW, Guo LW. Accelerated retinal ganglion cell death in mice deficient in the sigma-1 receptor. *Mol Vis.* 2011;17:1034–1043.
12. Jiang G, Mysona B, Dun Y, et al. Expression, subcellular localization and regulation of sigma receptor in retinal Müller cells. *Invest Ophthalmol Vis Sci.* 2006;47:5576–5582.
13. Ha Y, Dun Y, Thangaraju M, Ganapathy V, Smith SB. Sigma receptor 1 modulates ER stress in retinal neurons. *Invest Ophthalmol Vis Sci.* 2011;52:527–540.
14. Martin PM, Ola MS, Agarwal N, Ganapathy V, Smith SB. The sigma receptor ligand (+)-pentazocine prevents apoptotic retinal ganglion cell death induced in vitro by homocysteine and glutamate. *Mol Brain Res.* 2004;123:66–75.
15. Dun Y, Thangaraju M, Prasad P, Ganapathy V, Smith SB. Prevention of excitotoxicity in primary retinal ganglion cells by (+)-pentazocine, a sigma receptor-1 specific ligand. *Invest Ophthalmol Vis Sci.* 2007;48:4785–4794.
16. Smith SB, Duplantier JN, Dun Y, et al. In vivo protection against retinal neurodegeneration by the sigma receptor 1 ligand (+)-pentazocine. *Invest Ophthalmol Vis Sci.* 2008;49:4154–4161.
17. Tchedre KT, Huang RQ, Dibas A, et al. Sigma-1 receptor regulation of voltage-gated calcium channels involves a direct interaction. *Invest Ophthalmol Vis Sci.* 2008;49:4993–5002.
18. Zhang XJ, Liu LL, Jiang SX, Zhong YM, Yang XL. Activation of the sigma receptor 1 suppresses NMDA responses in rat retinal ganglion cells. *Neuroscience.* 2011;177:12–22.
19. Sabino V, Cottone P, Parylak SL, Steardo L, Zorrilla EP. Sigma-1 receptor knockout mice display a depressive-like phenotype. *Behav Brain Res.* 2009;198:472–476.
20. Moore P, El-Sherbeny A, Roon P, et al. Apoptotic retinal ganglion cell death is induced in vivo by the excitatory amino acid homocysteine. *Exp Eye Res.* 2001;73:45–47.

21. Bucolo C, Drago F, Lin LR, Reddy VN. Sigma receptor ligands protect human retinal cells against oxidative stress. *Neuroreport.* 2006;17:287–291.
22. Sieving PA, Frishman LJ, Steinberg RH. Scotopic threshold response of proximal retina in cat. *J Neurophysiol.* 1986;56:1049–1061.
23. Saszik SM, Robson JG, Frishman LJ. The scotopic threshold response of the dark-adapted electroretinogram of the mouse. *J Physiol.* 2002;543:899–916.
24. Seiji M, Iwashita S. On the site of melanin formation in melanocytes. *J Biochem Tokyo.* 1963;54:465–467.
25. May CA, Lütjen-Drecoll E. Morphology of the murine optic nerve. *Invest Ophthalmol Vis Sci.* 2002;43:2206–2212.
26. Howell GR, Libby RT, Jakobs TC, et al. Axons of retinal ganglion cells are insulted in the optic nerve early in DBA/2J glaucoma. *J Cell Biol.* 2007;179:1523–1537.
27. Ruiz-Ederra J, Garcia M, Hicks D, Vecino E. Comparative study of the three neurofilament subunits within pig and human retinal ganglion cells, *Mol Vis.* 2004;10:83–92.
28. Maurice T, Su TP. The pharmacology of sigma-1 receptors. *Pharmacol Ther.* 2009;124:195–206.
29. Langa F, Codony X, Tovar V, et al. Generation and phenotypic analysis of sigma receptor type I (sigma 1) knockout mice. *Eur J Neurosci.* 2003;18:2188–2196.
30. Cendán CM, Pujalte JM, Portillo-Salido E, Montoliu L, Baeyens JM. Formalin-induced pain is reduced in sigma(1) receptor knockout mice. *Eur J Pharmacol.* 2005;511:73–74.
31. Entrena JM, Cobos EJ, Nieto FR, et al. Sigma-1 receptors are essential for capsaicin-induced mechanical hypersensitivity: studies with selective sigma-1 ligands and sigma-1 knockout mice. *Pain.* 2009;143:252–261.
32. de la Puente B, Nadal X, Portillo-Salido E, et al. Sigma-1 receptors regulate activity-induced spinal sensitization and neuropathic pain after peripheral nerve injury. *Pain.* 2009;145:294–303.
33. Fontanilla D, Johannessen M, Hajipour AR, et al. The hallucinogen N,N-dimethyltryptamine (DMT) is an endogenous sigma-1 receptor regulator. *Science.* 2009;323:934–937.
34. Mavlyutov TA, Epstein ML, Andersen KA, Ziskind-Conhaim L, Ruoho AE. The sigma-1 receptor is enriched in postsynaptic sites of C-terminals in mouse motoneurons: an anatomical and behavioral study. *Neuroscience.* 2010;167:247–255.
35. Johannessen M, Ramachandran S, Riemer L, et al. Voltage-gated sodium channel modulation by sigma-receptors in cardiac myocytes and heterologous systems. *Am J Physiol Cell Physiol.* 2009;296:C1049–1057.
36. Frishman LJ, Wang MH. Electroretinogram of human, monkey and mouse. In: Levin LA, Nilsson SFE, Ver Hoeve J, Wu S, Kaufman PL, Alm A. *Adler's Physiology of the Eye*. 11th ed. New York: Saunders Elsevier; 2011:480–501.
37. Crish SD, Calkins DJ. Neurodegeneration in glaucoma: progression and calcium-dependent intracellular mechanisms. *Neuroscience.* 2011;176:1–11.
38. Clapham DE. Calcium signaling. *Cell.* 1995;80:259–268.
39. Simpson PB, Challiss RA, Nahorski SR. Neuronal Ca^{2+} stores: activation and function. *Trends Neurosci.* 1995;18:299–306.
40. Berridge MJ, Bootman MD, Lipp P. Calcium: a life and death signal. *Nature.* 1998;395:645–648.
41. Wu Z, Bowen WD. Role of sigma-1 receptor C-terminal segment in inositol 1,4,5-trisphosphate receptor activation: constitutive enhancement of calcium signaling in MCF-7 tumor cells. *J Biol Chem.* 2008;283:28198–28215.
42. Tchedre KT, Yorio T. Sigma-1 receptors protect RGC-5 cells from apoptosis by regulating intracellular calcium, Bax levels, and caspase-3 activation. *Invest Ophthalmol Vis Sci.* 2008;49:2577–2588.
43. Kim I, Xu W, Reed JC. Cell death and endoplasmic reticulum stress: disease relevance and therapeutic opportunities. *Nat Rev Drug Discov.* 2008;7:1013–1030.